J Nanostruct Chem (2016) 6:171–182
DOI 10.1007/s40097-016-0192-3

ORIGINAL RESEARCH

Preparation of nano-structured cryptomelane materials for catalytic oxidation reactions

S. Said[1] · M. Riad[1] · M. Helmy[1] · S. Mikhail[1] · L. Khalil[2]

Received: 24 February 2016 / Accepted: 31 March 2016 / Published online: 4 May 2016

Abstract Manganese-based octahedral molecular sieves of the type K-OMS-2 (cryptomelane structure) were prepared via reflux method by synproportionation of $KMnO_4$ and Mn^{2+} in acidic aqueous suspension. For this method, different manganese anions (sulphate, chloride and acetate) were used, which exert a strong influence on the prepared materials. Several techniques such as X-ray diffraction, Fourier transformer infrared, Raman spectroscopy, transmission electron microscopy, differential and gravimetric thermal analysis and H_2-temperature programmed reduction were used to characterize the prepared samples. The results revealed that the prepared samples were mainly pure mono-phase cryptomelane materials. The obtained K-OMS-2 material on using the sulphate anion has more available lattice oxygen as compared to that prepared by the other anions. The catalytic activity of the prepared samples was tested towards the oxidative dehydrogenation of cyclohexane. Over the K-OMS-2RS sample, cyclohexane conversion was significantly higher than the other prepared samples.

Keywords Octahedral molecular sieves · Manganese oxide · Cyclohexane · Catalytic oxidation reaction · Cyclohexene

✉ M. Riad
maryriad2006@yahoo.com

[1] Egyptian Petroleum Research Institute, Cairo, Egypt

[2] Faculty of Science, Ain Shames University, St. Cairo, Egypt

Introduction

Catalytic partial oxidation of hydrocarbons "particularly alkanes", using oxygen or air as oxidant, is significant and economical for the chemical industry. Among various alkane oxidations, the selective oxidation of cyclohexane is much attractive because of its formed product, cyclohexene.

Cyclohexene is used as an intermediate for the production of cyclohexanol, which is dehydrogenated to give cyclohexanone, a precursor to caprolactam. Caprolactam is the precursor to Nylon 6, a widely used synthetic polymer.

Cyclohexene is also a precursor to adipic acid, maleic acid, dicyclohexyl adipate, and cyclohexene oxide and can be used as a specific solvent. This reaction is operated in liquid phase using heterogeneous catalysts, but required high temperature (~150 °C), besides high selectivity (>80 %) to the sum of cyclohexanol and cyclohexanone only could be observed at low cyclohexane conversion [1]. Modi and Trivedi, [2] studied the catalytic behaviour of zeolite-Y-entrapped Ru(III) and Fe(III) complexes over the oxidation of cyclohexane forming cyclohexanone and cyclohexanol. Zeolite-Y-entrapped Ru showed higher catalytic activity (41.1 %) with cyclohexanone (84.6 %) selectivity. Therefore, the development of effective homogeneous catalysts could offer advantages.

Cryptomelane (K-OMS-2), an octahedral molecular sieve, is an allotropic form of manganese oxide having a well-defined tunnel structure. K-OMS-2 constructed from edge-shared double chains MnO_6 octahedra units that are corner connected to form an open tunnel of 4.6 by 4.6 A° size. Potassium ions are situated inside the tunnels to provide charge balance and to stabilize the structure (chemical composition = $KMn_8O_{16}.nH_2O$). The diameters of the tunnel cross sections are in the range of that for

typical zeolite pores. Due to its porous structure, hydrophobic nature, easy release of lattice oxygen, acidic sites and mixed valence of manganese species, low cost-efficient and environmentally friendly, cryptomelanes have been extensively explored for potential applications such as molecular sieves which are used as catalyst. They have gained a good performance in redox catalysis alternative to the conventional catalyst such as supported noble metals [3]. Several different morphologies have been synthesized, ranging from micrometer-long fibres to nanorods and paper-like materials [4].

Different methods have been reported for preparing K-OMS-2 such as: reflux [5] basic [6], reduction in the presence of surfactant [7] and sonication [8]. From these methods, a variety of cryptomelane materials were obtained with different morphology, crystallite size, evolution of lattice oxygen and enhanced activity in various oxidation processes.

Schurz et al. [9] prepared K-OMS-2 via the reflux method and studied the influence of cationic precursors $KMnO_4$ and $Ba(MnO4)_2$ on the synthesis product and tested for the oxidation of benzyl alcohol with molecular oxygen in liquid toluene at 110 °C. The catalytic activity of the K-OMS-2 is higher than Ba-OMS-2 materials, which directly correlated to their higher surface area.

Sithambarama et al. [10] prepared K-OMS-2 by the reflux method and investigated their activity for hydrogen generation via the water–gas shift reaction.

Sun et al. [11] prepared K-OMS-2 materials by solid-state and reflux methods to study the catalytic oxidation of toluene. The results established that K-OMS-2 prepared by the refluxing method exhibited higher catalytic activity than that by the solid-state reaction method. It was apparent that the high catalytic activity of the prepared K-OMS-2 prepared by the refluxing method attributed to the more available lattice oxygen and the higher oxygen mobility.

Deng et al. [12] prepared K-OMS-2 with different rod-like, fibrous-like and nest-like morphologies by solid-state reaction, reflux and hydrothermal methods, respectively. The materials were tested for liquid-phase oxidation of *p*-chlorotoluene to *p*-chlorobenzaldehyde. Over nest-like K-OMS-2, *p*-chlorotoluene conversion was significantly higher than that of the others.

Hndel et al. [13] prepared cryptomelane successfully at ambient pressure and temperature by a simple one-step reaction pathway based on redox reactions of either $MnSO_4$ or $MnCl_2$ together with $KMnO_4$ in aqueous solution.

Almquist et al. [14] prepared cryptomelane via three methods, reflux, milling and sol gel, and tested for ethanol oxidation. The results reveal that the sample prepared via the reflux method has the highest surface area compared to the other prepared samples and higher ethanol conversion.

Duan et al. [15] prepared (OMS-2) via reflux method and tested for the photodegradation of Acid Orange 7 in aqueous solutions; the catalyst shows enhanced activity and stability within the reaction time.

Accordingly, the common method for preparing K-OMS-2 is the reflux method, which has many advantages over the prepared cryptomelane materials such as redox property, oxygen vacancies, oxygen mobility and high surface area. These advantages resulted in the enhanced catalytic activity in different reaction processing.

In the current work, different K-OMS-2 materials were prepared via the reflux method. The diversity of the properties of the obtained materials depending on the type of anionic precursors including morphologies, crystallite size and lattice oxygen were investigated. The catalytic activity of the prepared samples towards oxidation reaction of cyclohexane was also recorded using flow system operated under atmospheric pressure.

Experimental

Preparation of K-OMS-2

K-OMS-2 was prepared through the oxidation of manganese sulphate by potassium permanganate in an acidic medium under reflux according to the procedure described by DeGuzman et al., [16]. A solution of 0.4 M potassium permanganate (13.3 g) was dissolved in 225 ml of distilled water at room temperature, and 6.7 ml of nitric acid (65 wt%) was added to adjust the pH value to "3.5". This solution was added to a second one consisting of 19.8 g $MnSO_4$ (1.75 M) dissolved in 67.5 ml of distilled water (under continuous stirring). The resulting solution was transferred to a 500 ml round-bottomed flask fitted with a reflux condenser, stirred vigorously and refluxed at a temperature of 100 °C for 24 h. The formed dark brown precipitate is filtered, washed until pH = 7 and then dried at 120 °C overnight. $MnSO_4.H_2O$ was replaced with either $MnCl_2.4H_2O$ or Mn $(CH_3OO)_2.4H_2O$, to investigate the influence of the anions on the texture and the structure of the prepared K-OMS-2 materials. The procedure is completed as described for manganese sulphate, except that for manganese acetate, the nitric acid is replaced by acetic acid. The prepared samples are denoted as K-OMS-2RS, K-OMS-2RC and K-OMS-2RA, respectively.

Structural phase changes

Different techniques were applied to investigate the physico-chemical characteristics of the prepared K-OMS-2 materials.

X-ray powder diffraction analysis (XRD)

The structure and phase purity of the prepared materials were analysed via X-ray diffraction (XRD). The experiments were carried out using a Shimadzu XD-1 diffractometer using Cu K_α radiation ($\lambda = 0.1542$ nm) at a beam voltage of 40 kV and 40 mA beam current.

The intensity data were collected at room temperature in a 2θ range of 10°–70° with a scan rate of 0.7 s^{-1}. The joint committee on Powder Diffraction Society (JCPDS) database was used to index the peaks of XRD.

Average crystallite size calculated from X-ray line broadening using Sherrer's equation at $2\theta = 37.5°$ characterized the prepared materials.

Fourier transformer infrared spectroscopy

Fourier transformer infrared (FTIR) spectroscopy experiments were performed on spectrometer Perkin-Elmer-Spectrum-1 in the range of 4000 to 400 cm^{-1} at a resolution of 4 cm^{-1}. The samples were ground to a fine powder and dispersed in KBr to compress into pellets before measurements.

Raman spectroscopy

Raman spectra were recorded at room temperature in the range of 100–800 cm^{-1} with an HR-UV 800 confocal scanning spectrometer (Horiba Jobin Yvon), equipped with a Peltier-cooled charge-coupled device (1152 × 298 pixels) with spectral resolution of 0.5 cm^{-1}. The Raman scattering was excited using a 632.81 nm excitation wavelength supplied by an internal He–Ne laser through an Olympus high-stability BXFM confocal microscope.

Thermal analysis

Differential thermal (DTA) and thermo-gravimetric (TG) analyses were performed to study the structural changes of the prepared materials with thermal treatment. A 10 mg of sample was heated up to 1100 °C, with a heating rate of 10 °C min^{-1} in an airflow at a rate of 50 ml min^{-1} on SDTQ-600 (TA-USA) thermo balance instrument.

High-resolution transmission electron microscope (HRTEM)

The morphologies of the prepared materials were studied using high-resolution transmission electron microscope (HRTEM). The images of the materials were obtained in JEOL JEM-2100F microscope operating at voltage of 200 kV. The samples were prepared by dispersing in ethanol and sonicated for 20 min. The suspension dropped on a carbon-coated copper grid for TEM observations.

Temperature-programmed reduction (TPR)

Temperature-programmed reduction experiments were carried out to investigate the redox properties (the ease of reducibility of metal oxide) for the studied materials. The experiments performed in automatic equipment (Chembet 3000, Quantachrome). Typically, 100 mg of calcined material was loaded into a quartz reactor and heated under inert atmosphere (20 ml/min N_2) at 200 °C for 3 h prior to running TPR experiments, and cooled down to room temperature in N_2. Then the sample was submitted to a constant rate of heat treatment (10 °C/min up to 1000 °C) in a gas flow (mixture H_2/N_2, 5/95 vol%, reducing gas) 80 ml/min. A thermal conductivity detector (TCD) employed to monitor the amount of hydrogen consumption.

Textural analysis

The textural properties were determined from the N_2 adsorption–desorption isotherms at liquid nitrogen temperature (−196 °C) and carried out using NOVA 3200 S Unite, automated gas sorption analyser (Quantachrome Corporation) system to investigate the textural properties of the prepared cryptomelane samples. All samples were degassed at 300 °C for 4 h in nitrogen atmosphere prior to adsorption to ensure a dry clean surface. The pore size distributions were determined from Barrett–Joyner–Halenda (BJH) method applied to the desorption branch of the isotherm.

Catalytic activity

The oxidation of cyclohexane was carried out in a fixed bed vertical downward flow glass reactor (internal diameter 6 mm), operated under atmospheric pressure. About 2 ml of the pretreated catalyst was placed at the hot zone of the reactor, supported on either side with a thin layer of quartz wool and ceramic beads. The reaction temperature was monitored by a thermocouple placed in the middle of the catalyst bed. The catalyst was activated at 250 °C for 2 h, before reaction in a controlled stream of air as a carrier gas with a flow rate of 50 ml min^{-1}. The cyclohexane reactant was fed into the reactor with the required flow rate (3 ml/h) using a syringe infusion pump. The collected products in the receiver flask were analysed in a gas chromatograph (Perkin-Elmer) equipped with a HP-1 capillary column (60 m × 0.32 mm × 0.5 μm) and a flame ionization detector.

Results and discussions

X-ray diffraction analysis (XRD)

X-ray diffraction patterns for the prepared K-OMS-2 material via the reflux method (using the different precursors) depicted in Fig. 1.

The pattern for the three different precursors reveals the appearance of diffraction peaks at $2\theta = 12.8°$, 18.5°, 28.9°, 37.5°, 42° and 50°; these peaks are consistent with those of the standard cryptomelane (K-OMS-2) material with tetragonal symmetry corresponding to KMn_8O_{16}, (JCPDS 29-1020), which emphasized that the resulting material is a cryptomelane structure.

The peak intensities are the apparent difference between the three studied precursors, which reflect a difference in the formed crystallite sizes. It seems to increase form sulphate to chloride and then drastically increases for acetate.

XRD for K-OMS-2RS exhibits two additional diffraction peaks at $2\theta = 21.53°$ and 46.03° (marked with asterisk in Fig. 1), with low intensity. Most likely, these peaks related to the more difficult paths for the elimination by calcination of sulphate compared to acetate and oxalate, indexed as K_2SO_4 [16].

The average crystallite sizes (Table 1) are in the order: K-OMS-2RC (26.6 nm) = K-OMS-2RS < K-OMS-2RA (30.4 nm), in parallel with the decrease in the size of the studied anions $Cl^- < SO_4^{-2} < CH_3COO^-$ and the decrease in the polarity $SO_4^{-2} > Cl^- > CH_3COO^-$. Thus, the acetate group has the largest size and the lowest polarity, which allows the cryptomelane particles to grow in large crystallite. Whereas sulphate and chloride species are difficult to eliminate compared to the acetate group and might be present as K_2SO_4 and $KClO_3$ [16], which induce the dispersion of the formed crystallites and prevent their agglomeration.

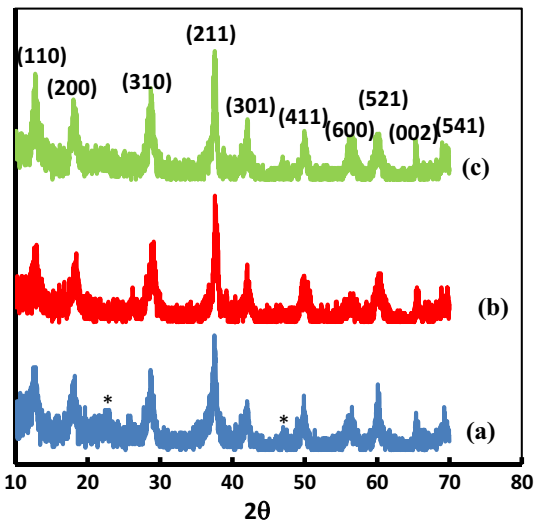

Fig. 1 The X-ray diffraction patterns of *a* OMS-2RS, *b* OMS-2RA, *c* OMS-2RC samples. *K_2SO_4

Fourier transformer infrared (FT-IR)

The FT-IR spectra for the prepared samples depicted in Fig. 2Aa–c. The spectrum detects several bands at 462, 516, 682, 1560 and 3362 cm^{-1} (on using sulphate anion), which are shifted to 455, 513, 671, 1584 and 3369 cm^{-1} (on using chloride anion) and to 458, 517, 677, 1568 and 3360 cm^{-1} (on using acetate anion). These bands ascribed to the vibrations of the MnO_6 octahedral framework, which present a clear signature of the cryptomelane structure [17].

The vibration band located at ~462 cm^{-1}, can be attributed to the vibration of the manganese species (Mn^{3+}) in the octahedral sites. The bands detected at ~517 and 682 cm^{-1} were assigned to the vibration due to displacement of the oxygen anions relative to the manganese ions along the direction of the octahedral chains, and the stretching mode of MnO_6 octahedral along the double chain, respectively. The band appeared at 1120 cm^{-1} is attributed to Mn–O–H, structural vibrations [18].

Meanwhile, the broadband detected at ~3369 cm^{-1} is assigned to the stretching vibration of the water molecule and OH^- in the lattice of the cryptomelane material, and that at ~1584 cm^{-1} is assigned to the bending vibration of water molecules in the tunnels and hydrogen-bounded OH-groups, which implies that the hydroxyl groups exist in the prepared material [19].

Raman spectroscopy

Raman spectroscopy for the prepared samples is depicted in Fig. 2Ba–c. The spectrum (K-OMS-2RS) reveals the appearance of Raman signals centred at 142, 250, 544 and 607 cm^{-1}. The peak detected at 544 cm^{-1} is assigned to the vibration that is due to the displacement of the oxygen anion (relative to manganese ion) along the direction of the octahedral chains, whereas the vibration frequency at 607 cm^{-1} is assigned to Mn–O stretching mode in tetrahedral sites environment, as confirmed by FT-IR. The signals at 142, 250 and 360 cm^{-1} are due to the Mn–O–Mn bending vibration in the MnO_2 octahedral lattice [20].

From Mn–O stretching range, the two sharp, high-intensity, high-frequency Raman bands at 544 and 607 cm^{-1} are indicative of a well-developed tetragonal structure with an interstitial space consisting of (2 × 2) tunnels of cryptomelane material [21, 22].

For OMS-2RC and OMS-2RA prepared materials the Raman signals for cryptomelane materials are shifted from 142, 167, 350, 569 and 622 to 155, 364, 557 and 611 cm^{-1}, respectively, as shown in Fig. 2Bb, c.

Table 1 The texture properties and weight loss of the prepared K-OMS-2R samples

Sample name	Textural parameters					Thermal behaviour				
	Crystallite size (nm)		S_{BET} (m^2/g)	$T{\cdot}V_p$ (cc/g)	D_p (nm)	Temperature ranges (°C)				Total Weight loss (%)
	XRD	TEM				25–250 (%)	300–750 (%)	750–950 (%)	950–1150 (%)	25–1150
K-OMS-2RS	26.6	9	96	0.3	12	5	6.6	0.99	2.6	*15.19*
K-OMS-2RC	26.6	8	68	0.2	3	4.93	5.42	3.05	3.08	*16.48*
K-OMS-2RA	30.4	11	86	0.2	3	3.67	4.66	2.55	2.53	*13.41*

Italic character is the total weight loss compared at different reaction temperature range

S_{BET} BET surface area, V_p pore volume, $T{\cdot}V_p$ total pore volume, D_p pore diameter

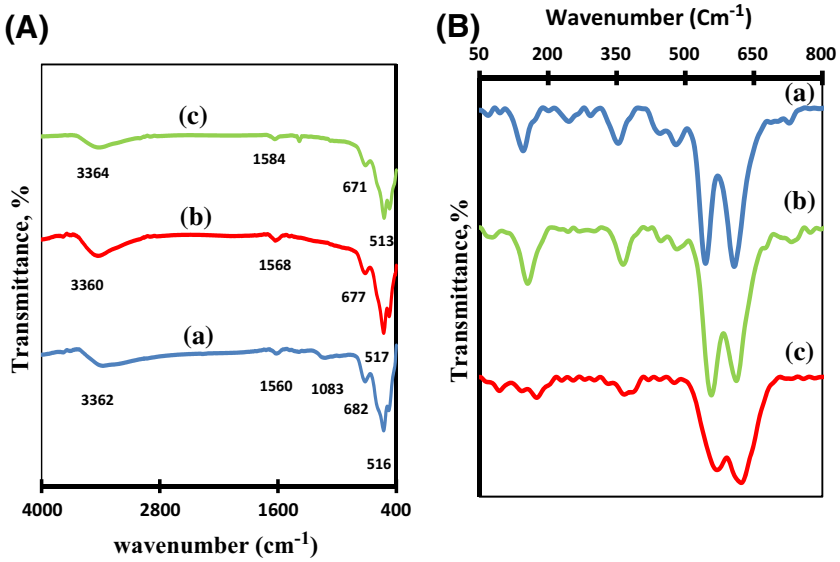

Fig. 2 **A** FT-IR, **B** Raman spectroscopy of *a* OMS-2RS, *b* OMS-2RA, *c* OMS-2RC samples

It is clear that the intensity of Raman bands at the range of 540–620 cm^{-1} increases from OMS-2RC to OMS-2RS and then OMS-2RA, which reveals a good tetragonal structure with an interstitial space consisting of (2 × 2) tunnels, developed for OMS-2RA compared with the other two samples.

In addition, the Raman signals are shifted to higher wave number in the order OMS-2RC > OMS-2RA > OMS-2RS, which implies that the material prepared using manganese sulphate precursor contains higher amounts of oxygen vacancies.

Differential and gravimetric thermal analysis (DTA and TGA)

Differential and gravimetric thermal analysis profiles for the prepared samples are represented in Fig. 3A–C.

The DTA profile (Fig. 3Aa) of K-OMS-2RS sample displayed three endothermic peaks located at 569, 849 and 967 °C "centred at 555, 855 and 969 °C, as confirmed from the dDTA profile". The endothermic peak at 569 °C is an indication for desorption of water inside the (2 × 2) tunnels, as stated by Suib [3]. The second and third endothermic peaks correspond to the phase transformation of MnO_2 into Mn_2O_3 and Mn_2O_3 into Mn_3O_4, respectively. The thermal behaviour for the K-OMS-2RC and K-OMS-2RA samples is the same as for K-OMS-2RS one, but shifted to higher temperatures 633, 879 and 1000 °C on using acetate, which implies its higher thermal stability.

These thermal effects were accompanied by steps of weight losses. The TG profile (Fig. 3Ab) demonstrates 5.0, 4.9 and 3.6 % weight losses, for sulphate, chloride and acetate materials, respectively, at the temperature range 25–250 °C, which could be due to the depletion of the physically and chemisorbed water molecules either on the surface and or on the channel structure. With the increase in the temperature to 750 °C, the weight loss increases to 6.6, 5.4 and 4.66 % (for K-OMS-2RS, K-OMS-2RC and K-OMS-2RA, respectively), which is due to the release of the water molecules inside the tunnels, besides the desorption of the structural oxygen close to the surface (related with the formation of lattice vacancies without

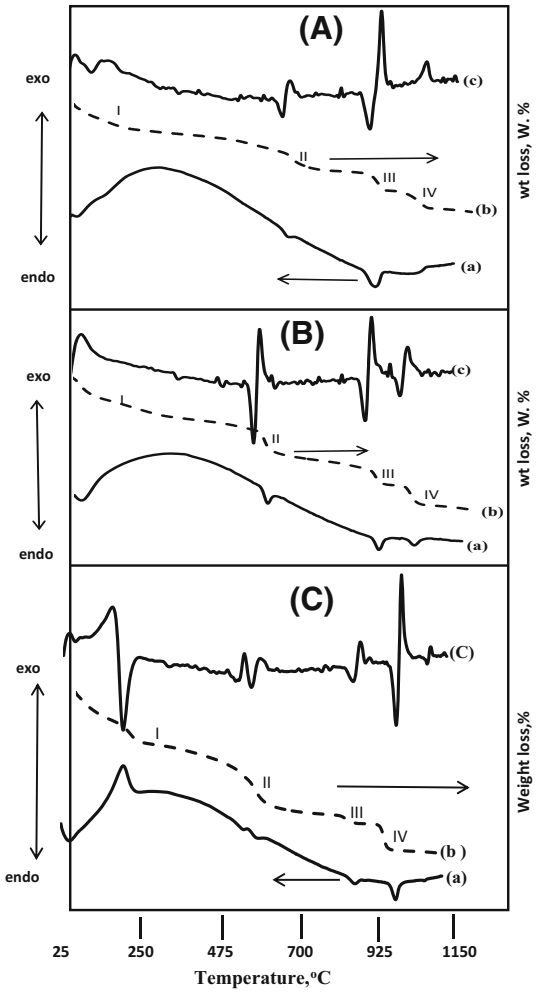

Fig. 3 *a* Differential thermal analysis (DTA), *b* thermal gravimetric analysis (TGA), *c* derivative differential thermal analysis (dDTA) of **A** K-OMS-2RS, **B** K-OMS-2RC, **c** K-OMS-2RA

decomposition of the material). A weight loss of ~1.0, 3.0 and 2.3 % at 750–950 °C, and 2.6, 3.1 and 2.5 % at up to 950 °C occurred on using K-OMS-2RS, K-OMS-2RC and K-OMS-2RA, respectively, which implies the transformation of cryptomelane to bixbyite (Mn_2O_3) and then to hausmannite (Mn_3O_4) species [23, 24], with total weight loss 15.20, 16.40 and 13.06 %. The total weight loss for acetate material (Fig. 3C) was found to be the lowest on "13.06" compared with the other ones, which indicates that K-OMS-2 material prepared on using the acetate anions was the most thermally stable one, in parallel with DTA behaviour.

Clearly, the weight losses at temperature range 250–750 °C are in the order sulphate > chloride > acetate. There are plenty of lattice oxygen in the produced OMS-2 material that prepared via the reflux technique on using manganese sulphate which become more easy to mobile upon thermal treatment (in agreement with the Raman spectroscopic results).

Transmission electron microscopy (TEM)

TEM was employed to investigate the morphologies of the prepared samples (Fig. 4a–c).

TEM image for nano-sized particles K-OMS-2RS material (Fig. 4a) shows agglomerated or clusters of disorderly stacked needle-like nanorods with an average diameter 9.0 nm. The TEM image for K-OMS-2RC (Fig. 4b) exhibits fine needle-like nanorod morphologies, which have regular shape in which their ends are similar in diameter as their middle part with an average diameter of 8.0 nm. Besides, the TEM image for K-OMS-2RA (Fig. 4c) shows dispersed needle-like crystallites, but with a larger average diameter of 11 nm. It is evident that the degree of dispersion for the prepared cryptomelane particles on using either acetate and or sulphate is higher than that on using chloride, in agreement with Walanda et al.'s [25] study.

H_2-Temperature programmed reduction (H_2-TPR)

H_2-temperature programmed reduction for the prepared samples is depicted in Fig. 5a–c.

H_2-TPR profile for OMS-2RS detects, two strong peaks at 383, 403 °C and the others are broad weak at 450, 650 °C, according to the postulated studies. These peaks related to the successive reduction steps as follows:

$$MnO_2 \rightarrow Mn_2O_3,$$

$$Mn_2O_3 \rightarrow Mn_3O_4,$$

$$Mn_3O_4 \rightarrow MnO,$$

$$MnO \rightarrow Mn^0.$$

As well known, the Mn–O bonds of K-OMS-2 are relatively weak and the Mn species in OMS-2 are reduced more easily at reduction temperature below 500 °C. Besides, Liu et al. [26] stated that due to the bigger negative reduction potential of MnO, no reduction band assignable to the $MnO \rightarrow Mn^0$ process was observed even up to 750 °C. Therefore, the weak reduction peak observed at 650 °C related to the reduction of some of K_2SO_4, which still inter-chelated in the cryptomelane structure [27]. Therefore, MnO was the final state of cryptomelane–MnO_2 reduction.

The TPR profile of K-OMS-2RC (Fig. 5b) is similar to that of sulphate, but the reduction peaks at 380 and 403 °C overlapped and appeared at 401 °C. Two reduction peaks were observed at 403 and 453 °C, the weak one at lower temperature is assigned to the reduction of MnO_2/Mn_2O_3 to Mn_3O_4, and the strong one at higher temperature is related to the reduction of Mn_3O_4 to MnO.

The H_2-TPR profile for the material prepared using manganese acetate as precursor (Fig. 5c) detected two

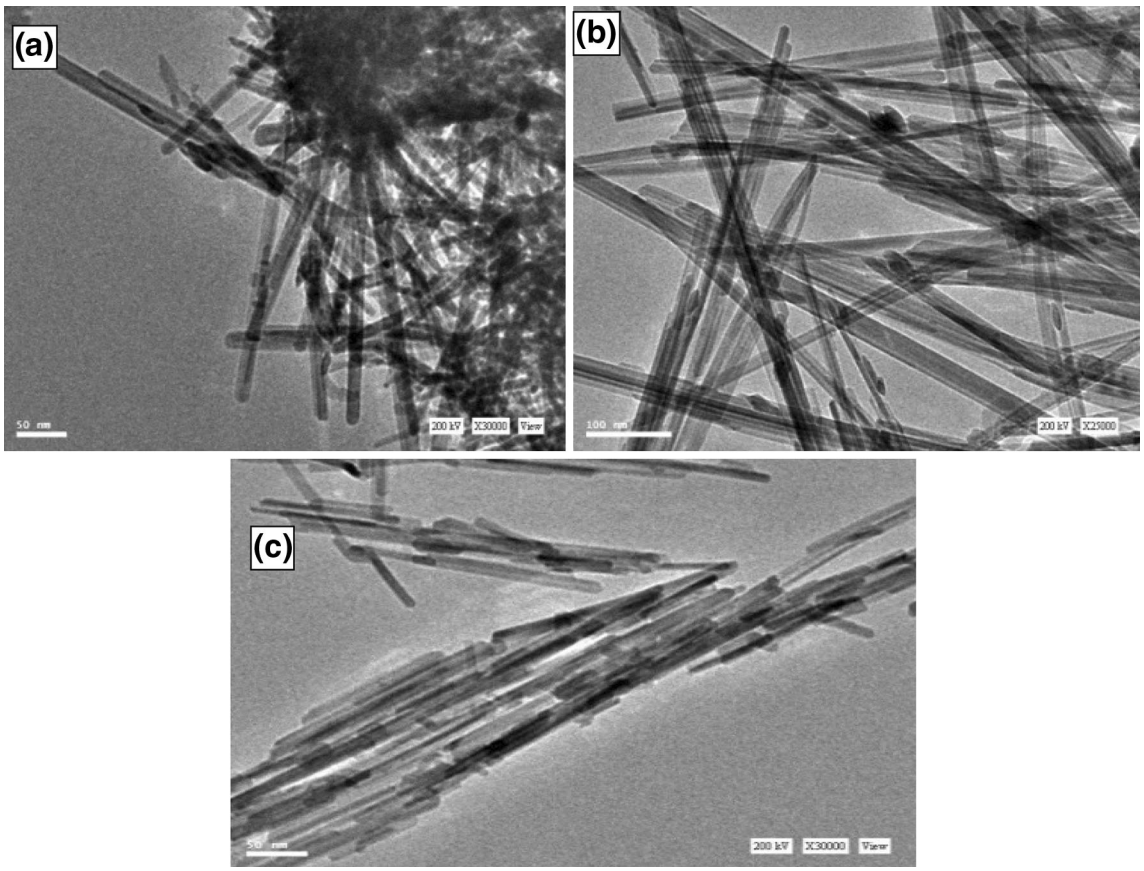

Fig. 4 TEM images of **a** OMS-2RS, **b** OMS-2RC, **c** OMS-2RA

reduction peaks at 349 and at 373 °C. The profile is similar to that using manganese sulphate and chloride, but the reduction peak (high temperature one) shifted to lower temperature from 450 to 375 °C compared with the two other precursors. This implies that the reduction of cryptomelane seems to be easier, i.e. the reducibility and reactivity of manganese are higher. In other words, the Mn–O bonds of OMS-2 on using manganese sulphate and manganese chloride precursors are stronger and reduced more difficultly than that for acetate.

Textural properties

The nitrogen adsorption–desorption isotherms (Fig. 6A) of the prepared K-OMS-2 needle-like nanorod samples show that the adsorption isotherms are related to type II according to Brunauer classification [28] and are characteristic for cryptomelane materials in accordance with Malinger et al. [29]. The isotherms of the samples exhibits H3-type hysteresis loop according to the IUPAC classification [30]. This type indicates the presence of the aggregation of plate-like nanoparticles giving rise to slit-shaped pores, due to the interparticle voids of the aggregated K-OMS-2 nanorods, in agreement with the TEM images (Fig. 4). The isotherm for K-OMS-2RS and K-OMS-2RA samples exhibited a hysteresis loop in a broader relative pressure range of $0.75 < P/P^0 < 1.0$, while the isotherm for K-OMS-2RC sample (Fig. 6A) reveals that the hysteresis loop nearly disappeared, suggesting the presence of capillary condensation without hysteresis taking place in the pores of the size range of wide micropores and/or narrow mesopores. Chloride anions can affect the morphology of the prepared OMS-2RC via either expansion and or contraction of the interconnectivity between nearby pores causing the disappearance of the hysteresis. The BJH pore size distribution curve derived from the desorption branch (Fig. 6B) reveals the presence of bimodal mesopores for the K-OMS-2RS and K-OMS-2RA samples. However, the bimodal distribution is not obvious for the K-OMS-2RC sample. These results reflect the role of large anionic precursor (sulphate and acetate) in the creation of heterogeneous pore size distribution in comparing with the small size chloride species.

The texture properties of the prepared samples are listed in Table 1. The surface area, total pore volume and average

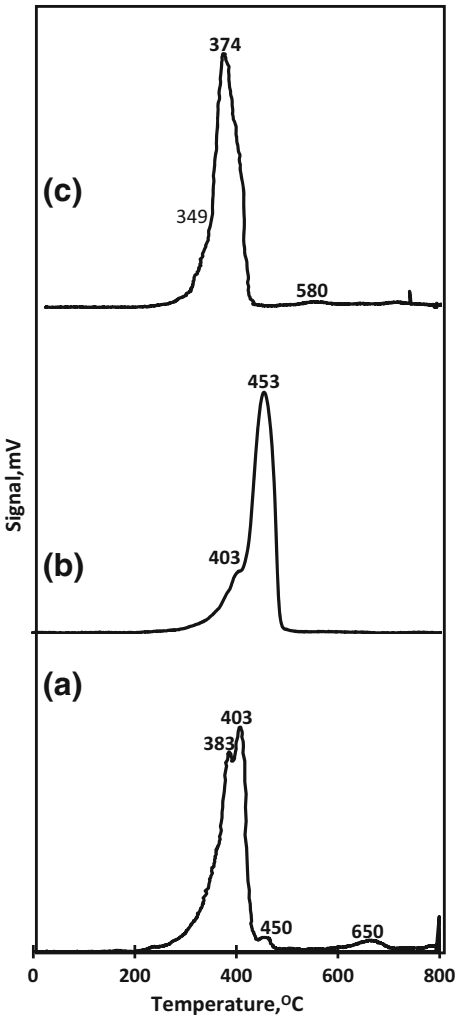

Fig. 5 TPR profiles of *a* OMS-2RS, *b* OMS-2RC and ©OMS-2RA samples

pore diameter of the K-OMS-2RS sample are 96 m^2 g^{-1}, 0.3 cm^3 g^{-1} and 12 nm respectively, which are higher than those of the K-OMS-2RC and K-OMS-2RA samples. These results match the XRD data (Fig. 1) and TEM images (Fig. 4) in terms of the particle size. The agglomeration of the needle-like nanorods forming bunches shows mesopores between the needles; this structure is responsible for the high surface area and total pore volume exposed by the K-OMS-2RS sample.

However, the high surface area value and the average pore diameter are shown to have a high value of 12.0 nm. This reflects the diffusion of the strong acidic sulphate species (large polar species) towards the narrow mesopores, allowing the opening up of some narrow regions to furnish a measurable area and expand the pores. Upon removing the sulphate species, it leaves behind pores with a relatively large diameter. Using the acetate group as precursor was able to increase the polarity of the K-OMS-2, and the adsorption of non-polar molecular N_2 hindered and decreased the measured BET area (86 g/cm^2).

The surface area for cryptomelane decreased on using chloride species as precursor compared with K-OMS-2RS, and becomes 68 m^2/g. This may be due to the accumulation of smaller particles of chloride species, which may still be contaminated with the formed cryptomelane material in the form of $KClO_3$ on the pore wall and opening, leading to a shrinkage in pore structure, a decrease in total pore volume and a significant drop in the extent of surface area. Thus, the surface area can widely vary depending on the type of the anion precursors.

Catalytic activity

The catalytic oxidation of cyclohexane is performed in a flow-type system operating under atmospheric pressure and at the reaction temperature varying between 300 and 400 °C, cyclohexane flow rate 3 ml/h, liquid hourly space velocity (LHSV = 1.5 h^{-1}) and with air flow rate of 50 ml/min. The results are illustrated in Figs. 7, 8 and 9.

From data in Fig. 7, it is clear that the total conversions for all samples increased with the increase in reaction temperature up to 400 °C. A low yield of liquid products obtained within the reaction temperature ranges 300–325 °C, and then sharply increases with further increase in the reaction temperature up to 400 °C. The amount of gaseous products slowly increased with increasing temperature from 300 to 400 °C.

The change in the activity of the prepared samples towards cyclohexane conversion is in the following sequence: K-OMS-2RS > K-OMS-2RC > K-OMS-2RA catalyst (histogram in Fig. 8).

From the liquid product distribution data obtained and given in Fig. 9, it is clear that the yield of the oxygenated products (cyclohexanon and cyclohexanal) increased with the increase in the reaction temperature. It exhibits low yield up to reaction temperature 350 °C, then the yield sharply increases with further increase in temperature and reaches its maximum value ~26 % at 400 °C on both K-OMS-2RS and K-OMS-2RC. Meanwhile, the OMS-2RA sample shows low yield towards the formation of oxygenated products.

On the other hand, the yield of the dehydrogenated products (cyclohexene) increased slightly with the gradual increase in the reaction temperature (for samples OMS-2RA and OMS-2RC) and low yield of dehydrogenated products obtained on raising the reaction temperature to 400 °C. For the sample OMS-2RS, the yield of dehydrogenated products show a maximum at the reaction temperature 350 °C (~46 %) and with a higher yield compared to the other two samples; then it decreases along with the increase in reaction temperature. The yield of

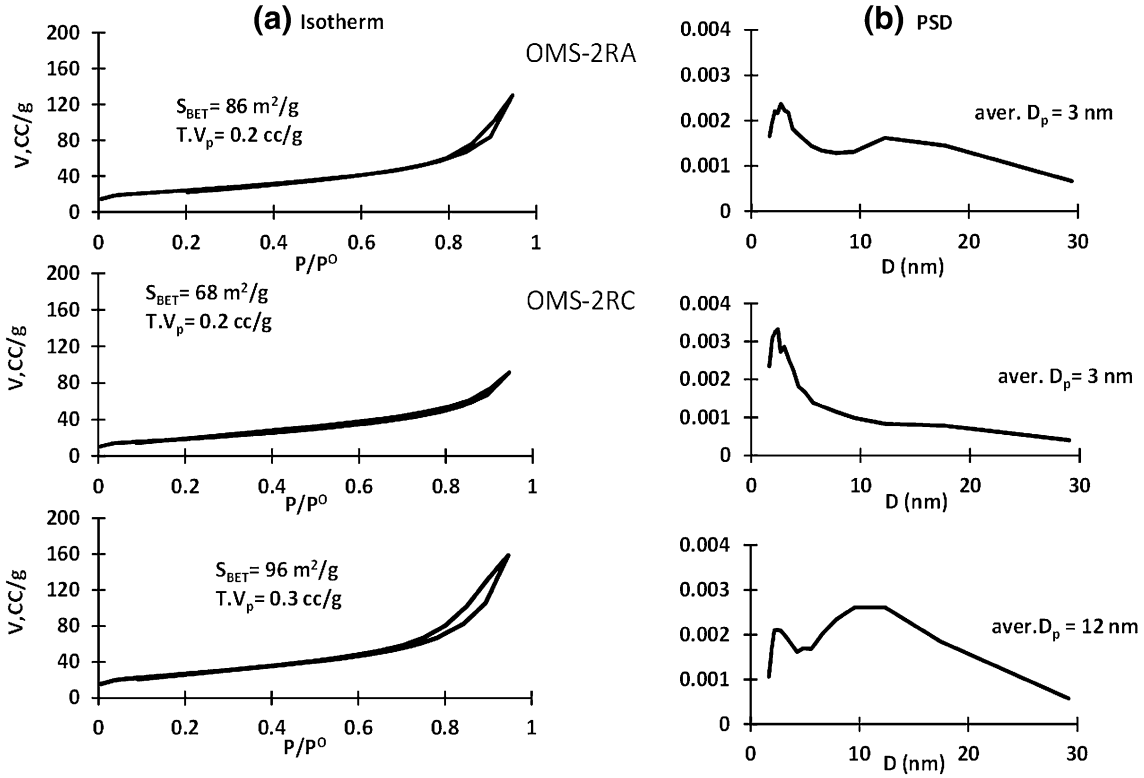

Fig. 6 **a** Nitrogen adsorption/desorption isotherms and **b** pore size distribution curves of K-OMS-2 samples

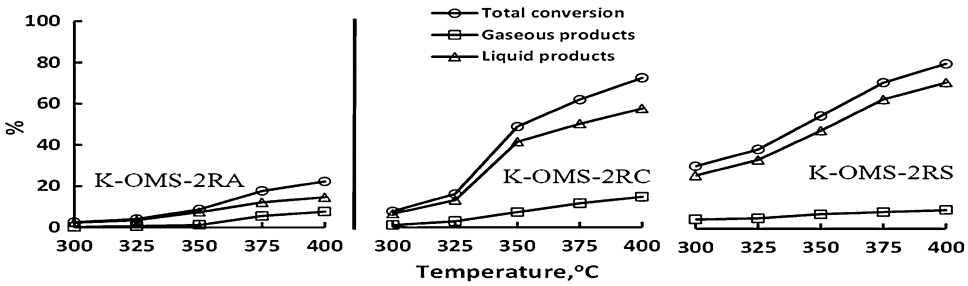

Fig. 7 Effect of reaction temperature on cyclohexane conversion over the K-OMS-2R samples

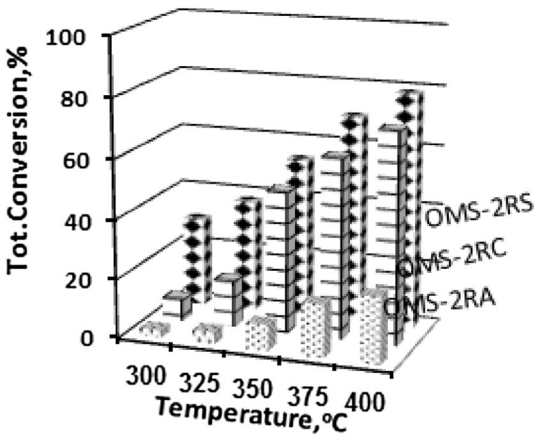

Fig. 8 The relation between the total conversion and the reaction temperature over the K-OMS-2R samples

alkylated and oxygenated products continue their increase with the gradual increase in reaction temperature, also with low yield for sample OMS-2RA (Fig. 9A).

Concurrently, the selectivity of the three prepared samples (OMS-2RA, OMS-2RS and OMS-2RC) towards the formation of the dehydrogenated products (cyclohexene) decreased with the increase in reaction temperature, which is parallel with the increase in the selectivity towards the formation of the alkylated products and also the oxygenated products (histogram in Fig. 9B). At temperature of 300°, OMS-2RS sample shows the highest selectivity towards the formation of cyclohexene, while OMS-2RC shows the highest selectivity for oxygenated products formation, in agreement with the results obtained by Abdel Dayem et al. [31], who prepared Ni/alumina catalyst doped with different rare earth metals and tested for cyclohexane

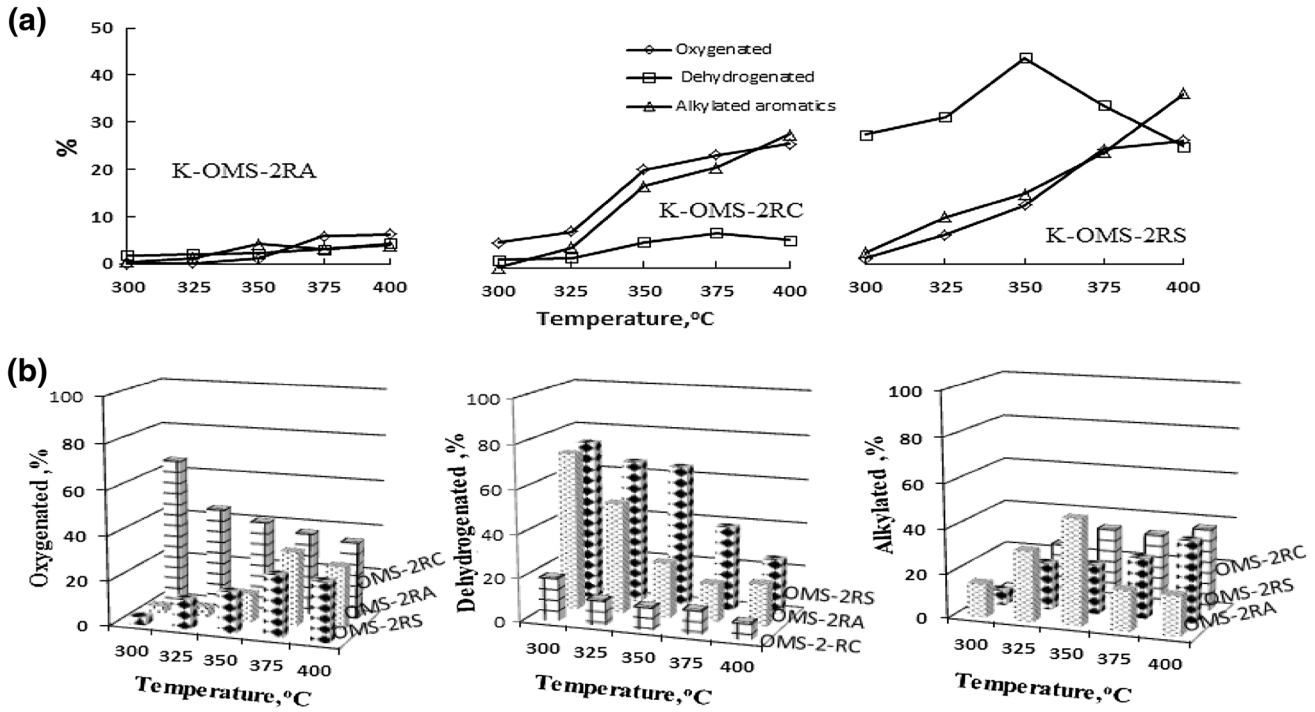

Fig. 9 Effect of reaction temperature on **a** the distribution and **b** the selectivity of the converted products over the K-OMS-2R samples

conversion, and Feng et al. [32], who prepared a series of manganese metalloporphyrins/ZnO and tested cyclohexane oxidation.

The high activity and selectivity of the OMS-2RS sample for cyclohexene formation at low and high temperature related to the high surface area allow the available active sites on the catalyst surface. Besides, high average pore diameter ~12 nm allows the easy desorption of cyclohexene intermediate before completing the oxidation reaction to oxygenated products. The small average diameter for OMS-2RC allows long residence time of the reactant on the active sites of the sample to complete its oxidation cycle to oxygenated products, besides the feasibility of lattice oxygen (as established from TPR results) which facilitates their contribution to the oxidation reaction and shows high selectivity and activity at low temperature.

Reaction mechanism

The mechanism proceeded as follows, in which adsorbed cyclohexane reacts with lattice oxygen and the reduced metal oxide reacts with adsorbed, dissociated oxygen. The oxidative dehydrogenation reaction mechanism is discussed as follows: gaseous oxygen participates in the reaction only after adsorption in other parts of the catalyst and then migrates through the lattice to the active sites by the re-oxidation between Mn^{3+} and Mn^{4+}. Mn^{4+}-O is responsible for providing the centre of oxidation for the adsorbed alkyl species, which contributes to a high conversion of cyclohexane, whereas Mn^{3+}–O is responsible for activating cyclohexane and adsorbing oxygen, which attributes a high selectivity to cyclohexene (oxidative dehydrogenated product).

Besides, the facility of oxygen dissociation occurred in metal-based catalyst by transferring an electron to metal centre, which is then back donated to the anti-bonding orbital of the molecule oxygen molecule. Cyclohexene is oxidized to cyclohexanol by the assistance of lattice oxygen and then dehydrogenated to cyclohexanon (oxygenated products).

Conclusion

Needle-like nanorods of cryptomelane-type manganese oxide K-OMS-2 nanomaterials were prepared via reflux of Mn^{+2} and Mn^{+7} in acidic medium using different manganese anions precursors (sulphate, chloride and acetate).

From the previous results, it was clarified that the nature of the anions played an important role in the structural characterization and the catalytic activity of the prepared cryptomelane sample as emphasized by the following.

The three different manganese anion precursors used for the preparation of the cryptomelanes produce a similar crystalline phase with minor differences in crystallite size and minor morphological variations coupled with different

nitrogen adsorptions in the three cryptomelane structures. The sample prepared using manganese acetate precursor contains the highest tunnel hydroxyl group and is a thermally stable one. The cryptomelane sample prepared using manganese sulphate as a precursor has more number of lattice oxygen species. In addition, the K-OMS-2RS sample exhibits high BET surface area, total pore volume and average pore diameter compared with the other two samples.

Although, K-OMS-2RA has the highest reducibility (as shown in TPR), it shows the lowest catalytic activity. The oxidation reaction of the cyclohexane is considered as a structure-sensitive reaction. The large pore diameter could be a reason why K-OMS-2RS was high in cyclohexane conversion. Besides, the loss of this oxygen creates nucleophilic vacancies in the lattice, implying their participation in the oxidation reaction of the cyclohexane.

References

1. Hattori, H., Ide, Y., Ogo, S., Inumaru, K., Sadakane, M., Sano, T.: Efficient and selective photocatalytic cyclohexane oxidation on a layered titanate modified with iron oxide under sunlight and CO_2 atmosphere. ACS Catal. **2**, 1910–1915 (2012)
2. Modi C, Trivedi P.: Zeolite-Y entrapped Ru(III) and Fe(III) complexes as heterogeneous catalysts for catalytic oxidation of cyclohexane reaction. Arab. J. Chem. 2013 (**Under press**)
3. Suib, S.: Porous manganese oxide octahedral molecular sieves and octahedral layered materials. Acc. Chem. Res. **41**, 479–487 (2008)
4. Peluso, M., Gambaro, L., Pronsato, E., Gazzoli, D., Thomas, H., Sambeth, J.: Synthesis and catalytic activity of manganese dioxide (type OMS-2) for the abatement of oxygenated VOCs. Catal. Today **133**, 487–492 (2008)
5. Dharmarathna, S., Kingóndu, C., Pahalagedara, L., Kuo, C., Zhang, Y., Suib, S.: Manganese octahedral molecular sieve (OMS-2) catalysts for selective aerobic oxidation of thiols to disulfides. Appl. Catal. B: Environ. **147**, 124–131 (2014)
6. Fan, C., Lu, A., Li, Y., Wang, C.: Synthesis, characterization, and catalytic activity of cryptomelane nanomaterials produced with industrial manganese sulphate. J. Colloid Interf. Sci. **327**, 393–402 (2008)
7. Tian, H., He, J., Zhang, X., Zhou, L., Wang, D.: Facile synthesis of porous manganese oxide K-OMS-2 materials and their catalytic activity for formaldehyde oxidation. Microporous Mesoporous Mater. **138**, 118–122 (2011)
8. Sun, H., Chen, S., Wang, P., Quan, X.: Catalytic oxidation of toluene over manganese oxide octahedral molecular sieves (OMS-2) synthesized by different methods. Chem. Eng. J. **178**, 191–196 (2011)
9. Schurz, F., Bauchert, J., Thorsten, M., Schleid, T., Hasse, H., Gläser, R.: Octahedral molecular sieves of the type K-OMS-2 with different particle sizes and morphologies: impact on the catalytic properties in the aerobic partial oxidation of benzyl alcohol. Appl. Catal. A: Gen. **355**, 42–49 (2009)
10. Sithambarama, S., Wenc, W., Njagia, E., Shenb, X., Hansonc, J., Suiba, S.: H_2 production through the water-gas shift reaction: an in situ time-resolved X-ray diffraction investigation of manganese OMS-2 catalyst. Catal. Today **156**, 2–7 (2010)
11. Sun, M., Yu, L., Ye, F., Diao, G., Yu, Q., Hao, Z., Zheng, Y., Yuan, L.: Transition metal doped cryptomelane-type manganese oxide for low-temperature catalytic combustion of dimethyl ether. Chem. Eng. J. **220**, 320–327 (2013)
12. Deng, Y., Zhang, T., Au, C., Yin, S.: Oxidation of p-chlorotoluene to p-chlorobenzaldehyde over manganese-based octahedral molecular sieves of different morphologies. Catal. Commun. **43**, 126–130 (2014)
13. Hndel, M., Rennert, T., Totsche, K.: Synthesis of cryptomelane- and birnessite-type manganese oxides at ambient pressure and temperature. J. Colloid Interf. Sci. **405**, 44–50 (2013)
14. Almquist, C., Krekeler, M., Jiang, L.: An investigation on the structure and catalytic activity of cryptomelane-type manganese oxide materials prepared by different synthesis routes. Chem. Eng. J. **252**, 249–262 (2014)
15. Duan, L., Sun, B., Wei, M., Luo, S., Pan, F., Xu, A., Li, X.: Catalytic degradation of Acid Orange 7 by manganese oxide octahedral molecular sieves with peroxymonosulfate under visible light irradiation. J. Hazard. Mater. **285**, 356–365 (2015)
16. DeGuzman, R., Shen, Y., Neth, E., Suib, S., O'Young, C., Levine, S., Newsam, J.: Synthesis and characterization of octahedral molecular sieves (OMS-2) having the hollandite structure. Chem. Mater. **6**, 815–821 (1994)
17. Gac, W.: The influence of silver on the structural, redox and catalytic properties of the cryptomelane-type manganese oxides in the low-temperature CO oxidation reaction. Appl. Catal. B: Environ. **75**, 107–117 (2007)
18. Julien, C., Massot, M., Poinsignon, C.: Profil enregistré d'une raie spectrale photographique et "largeur effective" Spectrochim. Acta A **60**, 689–694 (2004)
19. Hndel, M., Rennert, T., Totsche, K.: Synthesis of cryptomelane- and birnessite-type manganese oxides at ambient pressure and temperature. J. Coll. Interf. Sci. **405**, 44–50 (2013)
20. Chen, C., Njagi, Chen, S., Horvath, D., Morey, A., Mackin, C., Joesten, R., Suib, S.: Structural distortion of molybdenum-doped manganese oxide octahedral molecular sieves for enhanced catalytic performance. Inorg. Chem. **54**, 10163–10171 (2015)
21. Julien, C., Massot, M., Poinsignon, C.: Lattice vibrations of manganese oxides: part I. Periodic structures. Spectrochim. Acta A **60**, 689–700 (2004)
22. Lan, W., Chen, C.: Hybridization of graphene in 3D complex nanovoids: synergistic nanocomposites for electrocatalytic reduction of hydrogen peroxide. Electrochim. Acta **180**, 1014–1022 (2015)
23. Gao, T., Glerup, M., Krumeich, F., Nesper, R., Fjellvg, H., Norby, P.: Microstructures and spectroscopic properties of cryptomelane-type manganese dioxide nanofibers. J. Phys. Chem. C **112**, 13134–13140 (2008)
24. Cheng, F., He, C., Shu, D., Chen, H., Zhang, J., Tang, S.: Preparation of nanocrystalline VN by the melamine reduction of V_2O_5 xerogel and its supercapacitive. Mater. Chem. Phys. **131**, 268–273 (2011)
25. Walanda, D., Lawrance, G., Donne, S.: Hydrothermal MnO_2: synthesis, structure, morphology and discharge performance. J. Power Source **139**, 325–341 (2005)
26. Liu, X., Jin, Z., Lu, J., Wang, X., Luo, M.: Highly active CuO/OMS-2 catalysts for low-temperature CO oxidation. Chem. Eng. J. **162**, 151–157 (2010)

27. Kuo, C., Lan, W., Chen, C.: Redox preparation of mixed-valence cobalt manganese oxide nanostructured materials: highly efficient noble metal-free electrocatalysts for sensing hydrogen peroxide. Nanoscale **6**, 334–341 (2014)
28. Brunauer, S., Deming, S., Deming, E., Teller, E.: On a theory of the van der waals adsorption of gases. J. Am. Chem. Soc. **62**, 1723–1728 (1940)
29. Malinger, K., Ding, Y., Sithambaram, S., Espinal, L., Gomez, S., Suib, S.: Microwave frequency effects on synthesis of cryptomelane-type manganese oxide and catalytic activity of cryptomelane precursor. J. Catal. **239**, 290–298 (2006)
30. Gregg, S., Sing, K.: Adsorption surface area and porosity, 2nd edn. Academic Press Inc., London (1982)
31. Abdel Dayem, H., Faiz, M., Abdel-Samad, H., Hassan, S.: Rare earth oxides doped NiO/γ-Al_2O_3 catalyst for oxidative dehydrogenation of cyclohexane. J. Rare Earths **33**, 611–617 (2015)
32. Feng, Z., Xie, Y., Hao, F., Liu, P., Luo, H.: Catalytic oxidation of cyclohexane to KA oil by zinc oxide supportedmanganese 5, 10, 15, 20-tetrakis (4-nitrophenyl)porphyrin. J. Mol. Catal. A: Chem. **410**, 221–225 (2015)